This is the accepted version of an article published in Publication Geotechnical Testing Journal, A New Apparatus for Seepage and Internal Erosion Soil Column Tests in Geotechnical Centrifuge, Copyright © 2025, ASTM International, West Conshohocken, PA, pages 774–794, http://dx.doi.org/10.1520/GTJ20240182.

A New Apparatus for Seepage and Internal Erosion Soil Column Tests in Geotechnical Centrifuge

Authors: Chang Guo[1,2], Bo Huang[1,3]*, Jiying Fan[1,4], Wenyue Zhang[5], and Yao Tang[1,3]

[1] Institute of Geotechnical Engineering, College of Architectural and Civil Engineering, Zhejiang University, Hangzhou, China.

[2] Department of Civil and Environmental Engineering, The Hong Kong Polytechnic University, Hung Hom, Hong Kong.

[3] MOE Key Laboratory of Soft Soils and Geoenvironmental Engineering, Zhejiang University, Hangzhou, China.

[4] Geoengineering Centre at Queen's-RMC, Queen's University, Kingston, Canada.

[5] Formerly, Department of Civil and Environmental Engineering, Tokyo Institute of Technology, Tokyo, Japan; currently, Taisei Corporation, 344-1, Nase-cho, Tostuka-ku, Yokohama, Japan.

***Corresponding author**. E-mail: cehuangbo@zju.edu.cn

ABSTRACT

Understanding the hypergravity effect on seepage and internal erosion is the essential precondition for dam hydraulic disaster modeling using geotechnical centrifuges. Soil column testing is useful to bridge this knowledge gap, but previous attempts did not provide adequate functionality in centrifuge environments. This study develops a centrifuge-available apparatus for seepage and internal erosion soil column tests (CASIE). CASIE ensures a consistent and stable circulating water supply with no less than 34 000 ml/min at 80 *g* via double-bowl upstream and downstream water tanks and a vertical, multistage centrifugal pump. The hydraulic gradient can be controlled by adjusting the elevation of the upstream water tank using a servo lifting system with a vertical displacement range of 1.2 m and a maximum vertical speed of 155 mm/min. A rigid-wall permeameter is developed for multiple applications in soil column tests for seepage and internal erosion. The flowrate through the specimen can be measured using four parallel-installed oval gear flowmeters with a large measurement range of 10-10 000 ml/min. To validate the capabilities of CASIE, two suffusion (one form of internal erosion) tests were conducted at 1 *g* and 30 *g*. The results reveal that the scaling factor for the critical hydraulic gradient of 30 *g* to 1 *g* is 1/10. It is much less than the predicted value of 1, indicating that suffusion failure is more readily triggered in the hypergravity environment.

Keywords

Internal erosion, seepage, geotechnical centrifuge, soil column test, hypergravity effect, multi-functional apparatus

1 Introduction

Seepage-induced internal erosion, initiated by mechanisms such as concentrated leak, backward erosion piping, contact erosion, or suffusion, is a crucial factor in earth dam failure (Fell et al. 2003, Zhang et al. 2009, Bonelli and Nicot 2013, Fan and Rowe 2022). Compared to physical modeling at normal gravity (1 *g* = 9.8 m/s^2), geotechnical centrifuges can replicate the in-situ pressure field of full-scale prototypes in small-scale models by generating a hypergravity (*N* times of *g*, *N g*) environment (Taylor 1994, Huang et al. 2021). Hence, this technology is promising in predicting disasters of earth dams. However, the previous centrifuge modeling on internal erosion of dams revealed that hypergravity significantly lowers the critical hydraulic gradient initiating failure compared with semi-empirical predictions based on the experimental results at 1 *g* (van Beek and Zwanenburg 2010, Ovalle-Villamil and Sasanakul 2021). This discrepancy highlights the challenges in replicating the internal erosion process using geotechnical centrifuge models (Goodings 1982, Butterfield 2000, Hu et al. 2024, Wang et al. 2024). Hence, an improved understanding of the hypergravity effect on seepage-induced internal erosion is vital.

Soil column testing is an effective method for investigating the seepage and internal erosion behaviors of soils at 1 *g* (Terzaghi et al. 1995, Fannin and Moffat 2006, Moffat and Fannin 2006, Li 2008, Chang and Zhang 2011, Marot et al. 2024). It has also been applied in geotechnical centrifuges to study Darcy and non-Darcy flow permeability (Singh and Gupta 2000, van Tonder and Jacobsz 2017, Ovalle-Villamil and Sasanakul 2018), permeability of unsaturated soils (Zornberg and McCartney 2010), heave during the initiation phase of backward erosion piping (Ovalle-Villamil and Sasanakul 2020), and suffusion (Marot et al. 2012, Stevenson and Bowman 2025). However, the demanding condition within the centrifuge swinging basket limits the functions of the testing apparatus available at 1 *g*, impeding a deeper exploration of seepage and internal erosion behaviors (e.g., accurate measurement and quantitative prediction of the critical hydraulic gradient in different *g*-levels) in the hypergravity environment. This calls for a better-instrumented apparatus to achieve more realistic hydraulic and mechanical boundary conditions and monitor key hydraulic characteristics (e.g., flowrate and global and local hydraulic gradients) in the centrifuges.

There are two main challenges in developing the testing apparatus for seepage and internal erosion, as reviewed in Table 1. The first challenge is to ensure a continuous, stable, and controllable water supply to replicate the hydraulic conditions of engineering practice (e.g., cyclic hydraulic gradient due to waves (Chen and Zhang 2023)). Three solutions have been attempted. The first solution was using the falling-head method. For example, Singh and Gupta (2000) and van Tonder and Jacobsz (2017) performed centrifuge hydraulic conductivity tests by this method. Although this method is simple and effective for measuring soil permeability, the unstable and uncontrollable water supply limits further exploration of internal erosion behavior. The second solution involves centrifuge water supply lines which connect tubes from the centrifuge swinging basket to the ground through a fluid rotary joint (Taylor 1994, Zornberg and McCartney 2010, Kim et al. 2013, Shepley and Bolton 2013, Ovalle-Villamil and Sasanakul 2018, Ovalle-Villamil and Sasanakul 2020). For example, Ovalle-Villamil and Sasanakul (2018) used two centrifuge water supply lines to directly connect the input and output of the permeameter, forming a closed loop. Pneumatic tanks outside the centrifuge supplied high water pressure to soil specimens to study the high-speed non-Darcy flow in the hypergravity environment. However, this solution faces a limitation in the over-large hydraulic resistance from its over-long tubes, which would hinder the flexibility of hydraulic gradient control. The third solution was to achieve a water supply within the swinging basket (Wang et al. 2010, Marot et al. 2012, Stevenson and Bowman 2025).

For example, Marot et al. (2012) implemented a continuous circulating water supply in suffusion tests using a pump, with water levels maintained by an overflow tank. Stevenson and Bowman (2025) achieved a stable and controllable water supply in suffusion tests by utilizing an overflow upstream tank placed on a servo lifting table. This setup featured a pressurized supply tank to deliver water to the upstream tank and a collection tank to gather water from the downstream tank. The onset of suffusion was monitored through local and global potential energy gradients, measured by multiple pore pressure transducers (PPTs) on the permeameter sidewall. Although this solution shows promise, no apparatus has yet provided a water supply that simultaneously ensures continuity, stability, and controllability within the limited space of the centrifuge basket.

Another challenge is to measure the flowrate through specimens. Many flowmeters are not applicable in the centrifugal environment due to the limitation of working principles (e.g., Coriolis mass flowmeter) or the unsuitable measurement range and accuracy (e.g., electromagnetic flowmeter). Hence, previous studies normally resorted to indirect measurement techniques. For example, flowrates were estimated using the rate of water level change (Singh and Gupta 2000, van Tonder and Jacobsz 2017, Stevenson and Bowman 2025) or the displacement rate of pneumatic tank pistons in the experiments of Ovalle-Villamil and Sasanakul (2018). They are only suitable for their corresponding water supply solution, as mentioned before. Wang et al. (2010) utilized a triangular weir to evaluate the flowrate based on the theoretical relation between the flowrate and water height above the weir crotch. The accuracy of this method is not ideal due to the limited size of the model container and water level fluctuation, as they mentioned.

This paper introduces a new geotechnical centrifuge-available apparatus for seepage and internal erosion soil column tests (CASIE). CASIE provides enhanced capabilities, including a consistent and stable circulating water supply, a controllable hydraulic gradient, and multi-functional permeameters with a wide-range flowrate measurement. The performance of CASIE was examined through a series of calibration tests and two suffusion tests at 1 *g* and 30 *g*.

2 Description of CASIE

CASIE is developed for ZJU-400, a 400 *g*-ton beam geotechnical centrifuge at Zhejiang University, China. The centrifuge has a maximum acceleration of 150 *g* for static tests and an effective arm radius of 4.5 m. More details of this centrifuge can be found in Huang et al. (2021) and Fan et al. (2023). The main components of CASIE include a circulating water supply system, a servo lifting system, and instrumentations (see the apparatus layout in Fig. 1 and the photograph in Fig. 2). Further specific design details are outlined below.

2.1 Circulating water supply system with double-bowl water tanks

A circulating water supply system is designed to provide a consistent and stable water supply. The upstream and downstream tanks are placed on the servo lifting system and the centrifuge basket bottom plate, respectively. Each water tank is divided into a stabilizing bowl and an overflowing bowl via a partition (see Fig. 1). The stabilizing bowls are directly connected to the soil permeameter through the main tube (blue tube in Fig. 1). Water levels in stabilizing bowls are maintained by overflowing - any excess water in the stabilizing bowl overflows into the corresponding overflowing bowl through the partition. Consequently, the hydraulic gradient across the soil specimen can be controlled by adjusting the upstream water tank.

A drainage tube (orange tube in Fig. 1) is installed to drain water from the upstream overflow bowl to the downstream overflow bowl via gravity flow. Through the main tube or the drainage tube, water in the upstream stabilizing bowl finally flows into the downstream overflowing bowl. To achieve circular flow, a vertical, multistage centrifugal pump (Grundfos CR1-27 A-FGJ-A-E-HQQE) with a rated flowrate of 30 000 ml/min and a rated head of 128.3 m at 1 *g* is utilized to pump water back to the upstream stabilizing bowl. Excessive pumping is necessary for sustaining a continuous overflow in the upstream stabilizing bowl and maintaining the stability of the upstream water level. The performance of this pump in the hypergravity environment is verified later. Additionally, eroded soil particles risk damaging the pump and flowmeters. An upward L-shaped pipe is connected to the pump's inlet within the downstream overflow bowl to mitigate this risk. In the hypergravity environment, all eroded particles would settle at the bottoms of the stabilizing and overflow bowls in the downstream tank due to their increased weight. Furthermore, real-time video monitoring of the upstream tank, main tube, and permeameter confirms that no air bubbles enter the main tube and permeameters. This is because bubbles rise more easily in a hypergravity environment due to increased buoyancy.

2.2 Servo upstream lifting system with large load capacity and high precision

This system is designed to control the elevation of the upstream tank, thus regulating the hydraulic gradient across the soil specimen. It consists of a steel frame, a lifting table, four synchronized screw jacks, a servo motor, and various accessories (see Figs 1 and 2). The servo motor rotates the screws of the jacks to adjust the position of the upstream tank through traveling nuts. The safe load capacity of the lifting sub-system is 12 tons, sufficient for the 76 kg upstream water tank at 150 *g*. The maximum vertical movement range and the maximum vertical movement speed of the lifting table are 1.2 m with an accuracy of < 0.1 mm and 155 mm/min, respectively. Various hydraulic gradient paths (e.g., a cyclic hydraulic gradient (Chen and Zhang 2023)) can be applied via the servo control panel to replicate the hydraulic conditions of the engineering practice.

2.3 Multi-functional and multi-channel permeameter

A rigid-wall permeameter is designed in CASIE, consisting of a Perspex cylinder, a top cap, a base pedestal, an axial loading unit, and a pressure measurement unit. Different applications might need varying cylinder dimensions. The cylinder for suffusion tests in this study has an inner diameter of 100 mm, a wall thickness of 40 mm, and a height of 220 mm. The height of specimens examined herein is 150 mm. Openings are drilled along the cylinder sidewall at vertical intervals of 30 mm to monitor pore pressures along the specimen. The cylinder is fastened to the top cap and the base pedestal using four threaded rods with nuts. The axial loading unit comprises a perforated plate (Plate I), a loading rod, and multiple weights. The axial stress on the soil specimen can be controlled by adjusting the weights. The interior of the base pedestal is funnel-shaped, with a second perforated plate (Plate II) to support the soil. Teflon tape is wrapped around the side of Plate II to prevent dominant flow along the inner surface of the cylinder. In the subsequent suffusion tests, erosion was not observed to concentrate along the boundary wall during testing and while removing specimens, confirming the effectiveness of this method. This funnel and the space above the specimen are filled with gravel to prevent jet flow.

The pressure measurement unit is horizontally placed next to the permeameter for hydraulic pressure measurement. It has multiple parallel three-way-shaped connectors (see Fig. 4). One horizontal way of each connector is used to connect the hole on the cylinder sidewall, the other horizontal way is for embedding PPTs, and the remaining upward way is for gas release during tube saturation via a waterproof screw. The connectors can be attached to the openings on the cylinder sidewall via tubes (see Fig. 1). Compared to mounting PPTs on the cylinder sidewall, one advantage of utilizing this unit is that the samples and PPTs can be saturated independently. It can prevent the desaturation of PPTs during sample preparation and improve the efficiency of tests using a single set of sensors for different specimens. Moreover, the PPTs in the unit directly measure the piezometric pressure (P) at a chosen point, regarding the elevation of the unit as the reference datum. This enables an accurate determination of the hydraulic pressure drop (ΔP, the sum of hydrostatic pressure difference and pore pressure difference) between two points, and consequently, the hydraulic gradient or potential energy gradient. In contrast, if PPTs were to be installed on the sidewall of the permeameter to measure the pore pressure difference, the hydrostatic pressure difference would need to be estimated. Such estimation would be almost imprecise due to the variation of *g*-level across the height in the geotechnical centrifuge.

This permeameter facilitates multiple applications in seepage and internal erosion soil column testing, including, but not limited to, tests of permeability, heave, and suffusion. Fig. 3 illustrates four examples. Firstly, permeability tests can be conducted by covering the surface of the perforated Plates I and II with metal meshes that have apertures smaller than the particle size to prevent particle loss. Fig. 3 (a) illustrates the layout of downward seepage using Ports I and II as inlet and outlet, respectively. Upward seepage can also be achieved by reversing the outlet and inlet. Secondly, Fig. 3 (b) depicts the testing configuration for heave, a typical process of the initial phase of the backward erosion piping (Ovalle-Villamil and Sasanakul 2020). It usually occurs in internal-stable soils with uniform or broad gradation subjected to upward seepage, where the upward seepage stress reduces the resultant effective stress of the soil to zero (Terzaghi et al. 1995, Fannin and Slangen 2014). Hence, the specimen's top surface is exposed by removing Plate I and securing the loading rod. The upward flow is achieved by connecting the upstream and downstream to Ports II and I, respectively. Finally, Fig. 3 (c) and (d) display two typical setups for suffusion tests. Suffusion normally occurs in poorly graded soils where fine particles are transported by seepage flow (Fannin and Slangen 2014). Hence, to access fine particles, a coarse metal mesh is affixed to the surface of Plate II during the downward flow in Fig. 3(c) or Plate I during the upward flow in Fig. 3 (d), permitting the escape of fine particles. Constant axial stress can be achieved by using the axial loading unit, as in Fig.3 (c), while constant volume conditions can be achieved by fixing the loading rod, as in Fig. 3 (d).

Up to four permeameters can be connected in parallel to conduct multi-channel tests during a single centrifuge operation (see Fig. 2). Each permeameter can be installed on the baseplate shown in Fig. 2, equipped with an electric ball valve, allowing for sequential testing of specimens by manipulating the valves as needed.

2.4 Measurement of flowrate

Oval gear flowmeters are utilized in CASIE to measure the flowrate through the soil specimen. Considering the limited measurement range of one single flowmeter, four oval gear flowmeters with a measurement range of 10-100, 30-300, 100-1000, and 800-10000 ml/min, respectively, are connected in parallel. The accuracy of each flowmeter is 0.2% of the corresponding full scale. Each flowmeter is connected in series to an electric ball valve (see Fig. 1). By controlling these valves, the most suitable flowmeter can be selected, ensuring flowrate measurements across a wide flowrate range of 10-10000 ml/min during the tests. The calibration and performance of the gear flowmeters in the hypergravity environment are discussed later.

3 Calibration of Main Functions in the Hypergravity Environment

3.1 Calibration of centrifugal pump

To verify the centrifugal pump capability, simple calibration tests were performed. A network camera was positioned above the upstream tank to record the time duration (Δt) required to fill the upstream stabilizing bowl with a volume of V. The pumping flowrate can be determined using $V/\Delta t$. The calibration tests were executed at 30, 50, and 80 g, with pumping heights (H_{pump}) of 0.2, 0.45, and 0.7 m, respectively. Fig. 5 illustrates the relationship between specific energy ($g \cdot H_{\text{pump}}$, a crucial property to quantify pump capacity) and the pumping flowrate. The manufacturer suggests the solid line, along with its tolerance range. Although data with specific energy lower than 600 m^2/s^2 are not provided, the calibration results closely align with the extrapolation of the suggested curves. The pumping flowrate is more than 34 000 ml/min (equivalent to a velocity of 70 m/s in a soil column with an internal diameter of 100 mm), ensuring an adequate water supply in CASIE.

3.2 Calibration of flowmeters

The oval gear flowmeter mainly consists of two oval gears with fixed axes within an ‘8’-shaped chamber (see Fig. 6). Two gears divide the chamber into three cells: an inlet cell (I), an outlet cell (O), and a temporary water-carrying cell (T). During each half cycle of gears rotating, the differential pressure between cells I and O rotates the gears, transferring water from cell T into cell B, and forming a new temporary water-carrying cell in the other part of the ‘8’-shaped chamber. Each cycle of gears rotating triggers an electronic pulse sensor to generate a square wave signal. As the volume of the water-carrying cell T is constant, the flowrate is theoretically proportional to the frequency of the gear rotation, which can be calculated from the number of square wave signals. This proportional coefficient, defined as the sensitivity of the sensor (K), is theoretically equal to twice the volume of the water-carrying cell T (see Fig. 6 (a)).

However, in a hypergravity environment, deformation of the gears and axes may occur, leading to gaps between the gears and the chamber. A small amount of water might leak through the gaps, resulting in measurement inaccuracies. The deformation may increase the hydraulic resistance inside the cells, leading to a higher hydraulic pressure loss in the chambers and thus enhancing the leakage. Therefore, it is necessary to verify the accuracy of gear flowmeters in the hypergravity environment.

The calibration tests were conducted via the falling head method, as illustrated in Fig. 7. The pump was stopped after filling the upstream tank stabilizing bowl. The flowmeters were directly set between the upstream and downstream water tanks. By manipulating the upstream tank elevation and the connecting tube length, various flowrates from the upstream stabilizing bowl to the downstream stabilizing bowl would be achieved and measured via the flowmeters. The actual flowrate, Q_{real} (i.e., the rate of decline in the water volume within the upstream stabilizing bowl) can be expressed as

$$Q_{\text{real}} = \frac{dh}{dt} S \tag{1}$$

where h is the mobilized water level in the upstream tank stabilizing bowl, and S is the inner cross-sectional area of the upstream stabilizing bowl. To monitor h, a PPT was placed in the upstream stabilizing bowl to measure the hydrostatic pressure (p_t), and two accelerometers were set on the lifting table, and centrifuge bottom plate to measure the corresponding accelerations, $N_t g$ and $N_b g$, respectively (see Fig. 7). Given that the acceleration of one point in the centrifuge is proportional to the distance to centrifuge rotation center, the acceleration at h can be derived as

$$N_h = N_t - \frac{hN_b}{R} \tag{2}$$

where R is the distance from the rotation center to the centrifuge bottom plate. Subsequently, p_t can be integrated by

$$p_t = \int_0^h \rho_w N_h g dh = \rho_w N_t g (h - \frac{N_b h^2}{N_t R}) \tag{3}$$

h in the upstream stabilizing bowl was solved as

$$h = \frac{N_t}{N_b} R - \sqrt{\frac{N_t^2}{N_b^2} R^2 - \frac{p_t R}{\rho_w N_b g}} \tag{4}$$

Then, the actual flowrate Q_{real} can be back-calculated by combing Eqs (1) and (4).

Four flowmeters were tested at 10, 30, 50, and 80 g. The flowmeter of 10-100 ml/min was not calibrated at 80 g due to the difficulty of achieving such a flowrate range. Fig. 8 compares the actual flowrate Q_{real} by Equation (1) and the flowrate Q_{measured} by the flowmeters. The values of Q_{real} and Q_{measured} show good proportional relationships. The slopes of the Q_{real}-Q_{measured} proportional relationship of different flowmeters at varying g-levels are summarized in Table 2. These slopes are also equivalent to the ratios of sensitivity measured at $N g$ (K_{N}) to that suggested by the manufacturer (K_1), K_{N}/K_1. All values of K_{N}/K_1 are slightly larger than 1, indicating a slight underestimation of the real flowrate by oval gear flowmeters in the hypergravity environment. The measurement range shows a limited effect on K_{N}/K_1. With the g-level increasing, the slopes of the proportional fitting lines slightly increase from 1.069 to 1.120, demonstrating hypergravity increases the obstruction on the gear rotation. For more accurate measurement in the hypergravity environment, the values of sensitivity suggested by the manufacturer (K_1) should be modified as K_{N}, based on the average empirical coefficients at the corresponding g-level listed in Table 2.

4 Typical Experimental Material and Methodology using CASIE

4.1 Soil material

The testing soil was a type of river sand from a reservoir in Lingshou County, Hebei Province, China. Mineralogical analysis reveals that the predominant constituents of this sand are quartz, albite, and feldspar. Its finer particles contain a small amount of potassium amphibole, polysilicon lepidolite, and chlorite. Therefore, the darker fine particles make it easy to distinguish through images of soils. The raw materials were sieved, from which particles with sizes of 0.075-0.106, and 0.85-1.67 mm were mixed in a ratio of 3:7 (see particle size distribution curve in Fig. 9). This artificially rearranged material is recognized as a poorly graded sand (SP) based on the Unified Soil Classification System (USCS) soil classification (ASTM 2017), and is susceptible to suffusion according to the criteria by Kézdi (1979), Kenney and Lau (1985), and Burenkova (1993).

The target relative density was 90%. More details about the sand are summarized in Table 3.

4.2 Testing program

Two suffusion tests were conducted at 1 *g* and 30 *g*, respectively, to verify the feasibility of CASIE. A constant volume condition and upward flow were simulated, as illustrated in Fig. 3 (d). Four PPTs were used to measure No. 1, 2, 4, and 5 openings at the cylinder sidewall shown in Fig. 1. The measurement range of PPTs used at 1 *g* and 30 *g* were 0-50 kPa and 0-400 kPa, respectively, with a 0.2% full-scale accuracy.

4.3 Scaling factors and hydraulic gradient in centrifuge modeling

The scaling factors differ between the conventional centrifuge model used for simulating the behavior of geotechnical structures and the soil column specimens in CASIE, which assess hypergravity effects. The scaling factor for any parameter X is denoted in bold as $\boldsymbol{X}$ (i.e., $\boldsymbol{X} = X_{\mathrm{m}}/X_{\mathrm{p}}$, where X_{m} and X_{p} represent the values of X in the model at N *g* and the prototype at 1 *g*, respectively). In conventional centrifuge modeling of geotechnical structures like dams and levees, the model is scaled from its prototype at 1 *g*. Consequently, the scaling factor for length, $\boldsymbol{L}$, in the model is typically considered as N^{-1}, ensuring that the scaling factor for stress remains 1 at N *g*, thereby maintaining the similarity of the stress field in the scaled model. However, varying model geometry sizes at different *g*-levels are inconvenient for assessing hypergravity effects on seepage and internal erosion behavior (Ovalle-Villamil and Sasanakul 2020). This also leads to debates about centrifuge scaling factors for hydraulic gradient and seepage velocity (Stevenson and Bowman 2025). Therefore, this study adopts the method by Ovalle-Villamil and Sasanakul (2020), treating $\boldsymbol{L}$ as 1 to facilitate the analysis of hypergravity effects on suffusion. This results in the scaling factor for stress being equal to N at N *g*.

There are debates surrounding the hydraulic gradient in hypergravity environments in previous studies. The hydraulic gradient (i) is explicitly a geometric gradient, calculated as the ratio of the hydraulic head difference (ΔH) to the distance between two head locations (ΔL). Regardless of the value of $\boldsymbol{L}$, the scaling factor for the hydraulic head, $\boldsymbol{H}$, remains consistent with $\boldsymbol{L}$ at varying g-levels, making the scaling factor for the hydraulic gradient, $\boldsymbol{i}$, equal to 1. On the other hand, the hydraulic gradient implicitly represents potential energy loss across a soil element due to hydraulic friction, directly affecting seepage velocity. With a constant hydraulic head difference, i remains constant at varying g-levels, but potential energy loss scales up by a factor of N at N g, making the scaling factor for seepage velocity, $\boldsymbol{v}$, equal to N. Thus, Thusyanthan and Madabhushi (2003), Ovalle-Villamil and Sasanakul (2018), and Stevenson and Bowman (2025) introduced the concept of potential energy gradient, e, to replace the hydraulic gradient in centrifuge seepage and suffusion soil column tests. With a consistent e, seepage (within both Darcy and non-Darcy flow regimes) through an identical soil element does not vary with hypergravity (i.e., $\boldsymbol{v} = 1$).

Although indirectly related to seepage velocity, i remains advantageous due to its practicality. It represents the actual boundary conditions of geotechnical structure models, regardless of the value of L. Therefore, in the centrifuge modeling of internal erosion behavior of dams by van Beek and Zwanenburg (2010) and Ovalle-Villamil and Sasanakul (2021), i is still employed. Additionally, i is more directly related to the triggering condition of internal erosion (i.e., the critical hydraulic gradient, i_{cr}). Based on existing theories on heave and suffusion, the total seepage forces acting on particles and the total submerged weights of the particles reach equilibrium at the critical hydraulic gradient (Skempton and Brogan 1994, Terzaghi et al. 1995, Indraratna and Radampola 2002, Li and Fannin 2008, Li et al. 2024). According to the limit equilibrium analysis of a single particle by Indraratna and Radampola (2002), the seepage force, which is the sum of drag force and hydrostatic force, is proportional to seepage velocity in Darcy flow. Thus, the N-fold increase in seepage velocity under the same hydraulic gradient at N g results in an N-fold increase in seepage force. The particle's submerged weight also increases by a factor of N due to the N times gravity. This implies that within Darcy flow regimes, the ratio of seepage force at a consistent hydraulic gradient to average submerged particle weight remains constant at different g-levels. Therefore, the theoretical scaling factor for the critical hydraulic gradient should be 1, which is more straightforward compared to the theoretical scaling factor for the critical potential energy gradient of N.

Thus, the hydraulic gradient is preferred in the following discussion, with the potential energy gradient included for reference, calculated as

$$i = Ne = \Delta H_{\mathrm{measured}}/\Delta L \tag{5}$$

where $\Delta H_{\mathrm{measured}}=\Delta P/(\rho_w N g)$, ΔP is the hydraulic pressure drop measured by PPTs, and ρ_w is the water density.

4.4 Specimen preparation and testing procedure

The samples were prepared using the moist tamping method. It is a widely used method to prepare specimens in soil column tests for internal erosion (Chang and Zhang 2011, Ke and Takahashi 2014, Nguyen et al. 2019) because it effectively avoids the separation of coarse and fine particles. The sand was mixed with a moisture content of around 12% and compacted to the target relative density in ten 15-mm layers. Carbon dioxide was slowly supplied into the permeameter from the bottom (Port II) to the top (Port I). After 2 hours, Port II was connected to water with a hydraulic gradient of less than 0.05 for at least 24 hours. Subsequently, the pressure measurement unit was connected to the permeameter.

Before the test at 30 g, the applied water level difference between the upstream and downstream stabilizing bowls ($\Delta H_{\text{applied}}$) was set as 0 mm, and all the electric valves closed. Once a steady centrifugal acceleration of 30 *g* was achieved, the valve linked to the 30-300 ml/min flowmeter was activated. The hydraulic loading path at 30 *g* is illustrated in Fig. 10, where $\Delta H_{\text{applied}}$ was progressively increased from 0 mm to 755 mm over 30 loading stages. It is important to note that, due to the head loss in tubes, $\Delta H_{\text{applied}}$ is normally unequal to the real hydraulic head difference over the soil specimen ($\Delta H_{\text{measured}}$). Each stage ended once a stable flowrate was reached. When the flowrate approached approximately 200 ml/min or 900 ml/min, the flowmeter was switched to the one with a larger measurement range. This switch slightly influenced the readings of PPTs due to the varying hydraulic resistance of different flowmeters, but this did not impact the relationship between the hydraulic gradient and the flowrate. At around 84 minutes, the flowrate and hydraulic gradients did not increase obviously with the hydraulic gradient increasing (see Fig. 11), indicating a violent washout of fine particles. Hence, the test was stopped.

At 1*g*, it is hard to achieve a high hydraulic gradient by controlling the elevation of the upstream tank. Therefore, a pressure-controllable Mariotte's bottle, similar to the approach utilized by Chang and Zhang (2011), was employed as a substitute for the upstream tank. The air inlet tube was connected to a precision pneumatic regulator (SMC IR2000) and an air pump. The hydraulic gradient was controlled incrementally by adjusting the inlet air pressure.

5 Preliminary Results and Discussion

5.1 Suffusion process at different *g*-levels

Fig. 11 illustrates the evolution of the hydraulic gradient and flowrate at 30 *g*. The local gradients of Zone I, II, and III ($i_{4\text{-}5}$, $i_{2\text{-}4}$, and $i_{1\text{-}2}$, respectively) and the global gradient ($i_{\text{average}} = i_{1\text{-}5}$) are included. Fig. 12 decipts the photographs of one side of the soil specimen captured by a digital camera during the test at 30 *g*. Before the test, the color of the specimen in Fig. 12 (a) was uniform, representing a homogeneous distribution of fine and coarse particles. At the initial stage of the test, the hydraulic gradients over each zone in the soil specimen and the flowrate synchronously increased in a stair-step pattern over the loading stages. At around 6 minutes, the growth rate of the local hydraulic gradient in Zone I, $i_{4\text{-}5}$, slowed down (see Fig. 11 (a)). In this phase, slight movements of some fine particles around coarse particles were observed. $i_{4\text{-}5}$ reduced suddenly at 7 minutes, indicating the "onset of instability" in Zone I. This phenomenon is consistent with the results of Fannin and Moffat (2006) and Stevenson and Bowman (2025). After about 21 minutes, more coarse particles became distinguishable in the view of the permeameter's sidewall due to the loss of many fine particles (see Fig. 12 (b), 30*g*-2), with $i_{4\text{-}5}$ stabilizing around 0.7. The growth rate of $i_{2\text{-}4}$ also slowed down. During this period, the values of hydraulic gradients within each loading stage began to change obviously. $i_{4\text{-}5}$ and $i_{2\text{-}4}$ showed a decreasing trend, but $i_{2\text{-}4}$ was increasing. The flowrate also increased within each stage. It reveals a noticeable fine particle loss in Zone I and II. Around 37 minutes, some isolated small regions predominantly consisting of coarse particles appeared (Fig. 12 (c), 30*g*-3). Subsequently, these regions expanded in the following loading stages. Both $i_{2\text{-}4}$ and i_{average} approached a constant value of around 2, although the flowrate (Fig. 11 (b)) was increasing. Meanwhile, $i_{1\text{-}2}$ increased to around 3.7, and $i_{4\text{-}5}$ decreased to around 0.4 (Fig. 12 (d),30*g*-5). It indicates a drastic fine particle erosion and, thus, specimen failure.

The specimen tested at 1 *g* shows a similar evolution process to that observed at 30 *g* (see Fig. 13 (a)). At around 22 min, the "onset of instability" happened at Zone I. Subsequently, the growth rate of $i_{4\text{-}5}$ constantly reduced, and finally, $i_{4\text{-}5}$ began to decrease after the elapsed time of around 64 min. Meanwhile, $i_{2\text{-}4}$ kept pace with the increase of i_{average} but grew slower. This state remained until a sudden decrease of i_{average} at around 92 min, when the flowrate increased drastically, indicating the failure of the specimen.

Fig. 14 compares the relationship between the average hydraulic gradient, i_{average}, and the seepage velocity, v, at 1 and 30 g, where v is the flowrate divided by the specimen cross-sectional area. The hypergravity environment causes a limited effect on the shape of the v-i_{average} curve. Two curves started from the original point and initially displayed good linearity. During this process, the movement of fine particles might be only within void space, resulting in a linear v-i_{average} relationship. Subsequently, the seepage velocity increased disproportionately with the increase in hydraulic gradient, indicating further fine particle movement and local instability. The secant slope of the curves increased gradually until reaching an obvious cross-point, after which the velocity increased sharply with the v-i_{average} curve rising almost vertically. This cross-point (i.e., the critical hydraulic gradient) marked the violent washout of fine particles, as Skempton and Brogan (1994) described. The critical hydraulic gradient at 1 g is around 18, while that of 30 g equals 1.8. Correspondingly, the critical potential energy gradients at 1 and 30 g are around 18 and 54.

5.2 Preliminary discussion about hypergravity effect on suffusion

As demonstrated by the above results, the critical potential energy gradient at 30 g is 300% of that at 1 g. This is because, at 30 g, the seepage force under the critical potential energy gradient of 1 g remains almost unchanged due to the consistent seepage velocity, which is insufficient to overcome the higher particle weight. However, the critical hydraulic gradient at 30g is significantly lower than that at 1 g, with a measured scaling ratio of the critical hydraulic gradient between 30 g and 1 g around 1/10 less than the theoretical value of 1, suggesting that erosion is more likely to be triggered in the hypergravity environment. This might be related to the transition from Darcy to non-Darcy flow regimes. The seepage regime can be estimated using the Reynolds number, $Re = vd_{\mathrm{eff}}/\eta$, where η is the kinematic viscosity of the fluid in the porous medium, and d_{eff} is the effective particle size proposed by Carrier (2003). The effect of hypergravity on increasing seepage velocity can significantly expedite the transition to a non-Darcy seepage regime. Considering the continuous loss of fine particles during the suffusion process, the mean of the initial specimen's effective particle size and the coarse particle's effective particle size (0.712 mm) is used as d_{eff} to estimate the approximate seepage Reynolds number. Taking 1 as the critical Reynolds number that delineates Darcy from non-Darcy flow (Ovalle-Villamil and Sasanakul 2018, Ovalle-Villamil and Sasanakul 2020), the corresponding seepage velocity for the specific specimens in this study is 125.18×10^{-5} m/s. When the seepage velocity exceeds this value, the seepage regime is non-Darcy flow. As shown in Fig. 14, the demarcation lines of 125.18×10^{-5} m/s at 30g and 1g are at the i_{average} of 1.4 and 21.5, respectively. The former is lower than its critical hydraulic gradient, indicating significant erosion in non-Darcy flow conditions. In contrast, the latter exceeds its critical hydraulic gradient, suggesting a limited effect of non-Darcy flow. Most previous soil column testing at 1 g ensures that the seepage is within Darcy flow regime (Moffat and Fannin 2006, Ke and Takahashi 2014, Hunter and Bowman 2018). However, the acceleration effect of hypergravity on seepage velocity may make the flow regime transitions difficult to ignore or avoid in centrifuge modeling. In non-Darcy flow, the drag force increases more rapidly with rising seepage velocity compared to the linear increase in Darcy flow (Morrison 2013). Therefore, erosion under non-Darcy flow is more aggressive, resulting in a smaller critical hydraulic gradient, which limits the similarity of centrifuge modeling.

To ensure similarity in future centrifuge models of dams or levees, replacing water with a fluid of higher viscosity or reducing the particle size are potential solutions, as suggested by the scaling law discussions of Goodings (1982) and Butterfield (2000). Further soil column tests using CASIE are planned in both Darcy and non-Darcy flow regimes to fully understand the effects of hypergravity on internal erosion behaviors. The goal is to develop a scaling law for the design of centrifuge modeling of geotechnical structures and to aid in the interpretation of the modeling results.

6 Summaries and Conclusions

This study introduces a new multi-functional apparatus, CASIE, designed for conducting seepage and internal erosion tests via soil column tests in geotechnical centrifuges. CASIE aims to explore the hypergravity effects on soil seepage and internal erosion behaviors.

CASIE facilitates a continuous and steady circulating water supply for the soil column in the centrifuge environment using upstream and downstream water tanks with stabilizing and overflowing bowls and a vertical, multistage centrifugal pump. The water supply flowrate at 80 *g* is not less than 34 000 ml/min, sufficient for testing requirements. The hydraulic gradient across the soil specimen can be controlled by adjusting the elevation of the upstream water tank via a servo lifting system. The maximum vertical displacement and the maximum vertical speed of the servo lifting system are 1.2 m and 155 mm/min, respectively.

A rigid wall permeameter is developed to conduct soil column tests in various applications (e.g., seepage, heave, and suffusion) in CASIE. Up to four permeameters can be connected in parallel, allowing multi-channel tests during a single centrifuge operation. Oval gear flowmeters were proven to measure the flowrate through the specimen in the hypergravity environment. Four flowmeters connected in parallel ensure a broad measurement capacity spanning from 10-10000 ml/min. The sensitivities of the flowmeters were recalibrated in the hypergravity environment.

Preliminary suffusion tests conducted at 30 *g* and 1 *g* revealed that the erosion evolution process was similar at these two different *g*-levels. The hypergravity did not affect the curve shape of the velocity-hydraulic gradient relationship. However, the scaling factor for the critical hydraulic gradient between 30 *g* and 1 *g* measured in the preliminary tests was only 1/10, remarkably lower than the theoretical prediction of 1. It suggests that suffusion can be triggered more readily in the hypergravity environment. This might be related to the accelerated transition from Darcy to non-Darcy flow regime due to the *N*-fold increase in the seepage velocity rate at *N g*. Further experiments are expected to explore the hypergravity effects on seepage and internal erosion behaviors using CASIE to establish a scaling law for centrifuge physical modeling design.

Declaration

Competing Interests: The authors declare no competing interests.

Acknowledgments

The work presented in this article was supported by the Natural Science Foundation of Zhejiang Province (grant number LCZ19E080002) and the National Natural Science Foundation of China (Grant No. 51988101).

References

ASTM. 2017. *Standard practice for classification of soils for engineering purposes (unified soil classification system).* ASTM D2487-17(2025). West Conshohocken, PA, US: ASTM International, approved https://doi.org/10.1520/d2487-17r25

Bonelli, S. and F. Nicot. 2013. *Erosion in Geomechanics Applied to Dams and Levees*, Hoboken: John Wiley & Sons, Inc. https://doi.org/10.1002/9781118577165

Burenkova, V. 1993. "Assessment of suffusion in non-cohesive and graded soils." In *Filters in geotechnical and hydraulic engineering*, edited by Brauns, and Schüler, 357-360. Rotterdam: Balkema.

Butterfield, R. 2000, "Scale-Modelling of Fluid Flow in Geotechnical Centrifuges." *Soils and Foundations* 40, no. 6: 39-45. https://doi.org/10.3208/sandf.40.6_39

Carrier, W. D. 2003, "Goodbye, Hazen; Hello, Kozeny-Carman." *Journal of Geotechnical and Geoenvironmental Engineering* 129, no. 11: 1054-1056. https://doi.org/10.1061/(ASCE)1090-0241(2003)129:11(1054)

Chang, D. S. and L. M. Zhang. 2011, "A Stress-controlled Erosion Apparatus for Studying Internal Erosion in Soils." *Geotechnical Testing Journal* 34, no. 6. https://doi.org/10.1520/GTJ103889

Chen, C. and L. Zhang. 2023, "Hydro-mechanical behaviour of soil experiencing seepage erosion under cyclic hydraulic gradient." *Géotechnique* 73, no. 2: 115-127. https://doi.org/10.1680/jgeot.20.P.340

Fan, J. and R. K. Rowe. 2022, "Piping of silty sand tailings through a circular geomembrane hole." *Geotextiles and Geomembranes* 50, no. 1: 183-196. https://doi.org/10.1016/j.geotexmem.2021.10.003

Fan, J., X. Zhao, J. Liu, and B. Huang. 2023, "Seismic response of buried pipes in sloping medium dense sand." *Soil Dynamics and Earthquake Engineering* 170, no. 1: 107867. https://doi.org/10.1016/j.soildyn.2023.107867

Fannin, R. J. and R. Moffat. 2006, "Observations on internal stability of cohesionless soils." *Géotechnique* 56, no. 7: 497-500. https://doi.org/10.1680/geot.56.7.497

Fannin, R. J. and P. Slangen. 2014, "On the distinct phenomena of suffusion and suffosion." *Géotechnique Letters* 4, no. 4: 289-294. https://doi.org/10.1680/geolett.14.00051

Fell, R., C. F. Wan, J. Cyganiewicz, and M. Foster. 2003, "Time for Development of Internal Erosion and Piping in Embankment Dams." *Journal of Geotechnical and Geoenvironmental Engineering* 129, no. 4: 307-314. https://doi.org/10.1061/(ASCE)1090-0241(2003)129:4(307)

Goodings, D. J. 1982, "Relationships for centrifugal modelling of seepage and surface flow effects on embankment dams." *Géotechnique* 32, no. 2: 149-152. https://doi.org/10.1680/geot.1982.32.2.149

Hu, Y., W. Xu, Y. Chen, L. Zhan, R. Chen, Q. Li, C. Guo, J. Li, D. Zhuang, and Z. Jin. 2024, "Experimental Study on the Influence of Hypergravity on the Nonlinear Flow Behaviour in Rock Fracture." *Rock Mechanics and Rock Engineering* 57, no. 2: 961-978. https://doi.org/10.1007/s00603-023-03589-5

Huang, B., J. Liu, J. Fan, and D. Ling. 2021, "Experimental Study on Uplift Mechanisms of Pipes Buried in Sloping Medium Dense Sand." *Journal of Pipeline Systems Engineering and Practice* 12, no. 3: 04021027. https://doi.org/10.1061/(ASCE)PS.1949-1204.0000567

Hunter, R. P. and E. T. Bowman. 2018, "Visualisation of seepage-induced suffusion and suffosion within internally erodible granular media." *Géotechnique* 68, no. 10: 918-930. https://doi.org/10.1680/jgeot.17.P.161

Indraratna, B. and S. Radampola. 2002, "Analysis of Critical Hydraulic Gradient for Particle Movement in Filtration." *Journal of Geotechnical and Geoenvironmental Engineering* 128, no. 4: 347-350. https://doi.org/10.1061/(ASCE)1090-0241(2002)128:4(347)

Ke, L. and A. Takahashi. 2014, "Triaxial Erosion Test for Evaluation of Mechanical Consequences of Internal Erosion." *Geotechnical Testing Journal* 37, no. 2: 347-364. https://doi.org/10.1520/gtj20130049

Kenney, T. C. and D. Lau. 1985, "Internal stability of granular filters." *Canadian Geotechnical Journal* 22, no. 2: 215-225. https://doi.org/10.1139/t85-029

Kézdi, A. 1979. *Soil Physics: Selected Topics*, New York: Elsevier Publishing Company.

Kim, D. S., N. R. Kim, Y. W. Choo, and G. C. Cho. 2013, "A newly developed state-of-the-art geotechnical centrifuge in Korea." *KSCE Journal of Civil Engineering* 17, no. 1: 77-84. https://doi.org/10.1007/s12205-013-1350-5

Li, M. "Seepage Induced Instability in Widely Graded Soils." PhD Thesis, University of British Columbia, 2008. https://dx.doi.org/10.14288/1.0063080

Li, M. and R. J. Fannin. 2008, "Comparison of two criteria for internal stability of granular soil." *Canadian Geotechnical Journal* 45, no. 9: 1303-1309. https://doi.org/10.1139/t08-046

Li, M., R. J. Fannin, M. Foster, and L. Yan. 2024, "Internal instability of cohesionless soils in upward and downward flow: an experimental verification of theory." *Canadian Geotechnical Journal* 61, no. 9 (2024/09/01): 2036-2041. https://doi.org/10.1139/cgj-2023-0011

Marot, D., V. D. Le, J. Garnier, L. Thorel, and P. Audrain. 2012, "Study of scale effect in an internal erosion mechanism: centrifuge model and energy analysis." *European Journal of Environmental and Civil Engineering* 16, no. 1: 1 - 19. https://doi.org/10.1080/19648189.2012.667203

Marot, D., B. Oli, F. Bendahmane, R. Gelet, and P. Leroy. 2024, "A Hydraulic Gradient and Stress-Controlled Erosion Apparatus for Assessing Soil Internal Erosion." *Geotechnical Testing Journal* 47, no. 6. https://doi.org/10.1520/GTJ20230454

Moffat, R. and R. J. Fannin. 2006, "A Large Permeameter for Study of Internal Stability in Cohesionless Soils." *Geotechnical Testing Journal* 29, no. 4: 273-279. https://doi.org/10.1520/gtj100021

Morrison, F. A. 2013. *An introduction to fluid mechanics*, London: Cambridge University Press.

Nguyen, C. D., N. Benahmed, E. Andò, L. Sibille, and P. Philippe. 2019, "Experimental investigation of microstructural changes in soils eroded by suffusion using X-ray tomography." *Acta Geotechnica* 14, no. 3: 749 - 765. https://doi.org/10.1007/s11440-019-00787-w

Ovalle-Villamil, W. and I. Sasanakul. 2018. "A new insight into the behaviour of seepage flow in centrifuge modelling." In *Physical Modelling in Geotechnics, Volume 1*, edited by A. McNamara, S. Divall, R. Goodey, N. Taylor, S. Stallebrass, and J. Panchal, 259-264. London: CRC Press. https://doi.org/10.1201/9780429438660

Ovalle-Villamil, W. and I. Sasanakul. 2020, "Assessment of centrifuge modelling of internal erosion induced by upward flow conditions." *International Journal of Physical Modelling in Geotechnics* 21, no. 5: 1-17. https://doi.org/10.1680/jphmg.20.00004

Ovalle-Villamil, W. and I. Sasanakul. 2021, "Centrifuge Modeling Study of Backward Erosion Piping with Variable Exit Size." *Journal of Geotechnical and Geoenvironmental Engineering* 147, no. 11: 04021114. https://doi.org/10.1061/(ASCE)GT.1943-5606.0002642

Shepley, P. and M. D. Bolton. 2013, "Water supply to a geotechnical centrifuge." *International Journal of Physical Modelling in Geotechnics* 13, no. 3: 99-110. https://doi.org/10.1680/ijpmg.13.00001

Singh, D. N. and A. K. Gupta. 2000, "Modelling hydraulic conductivity in a small centrifuge." *Canadian Geotechnical Journal* 37, no. 5: 1150-1155. https://doi.org/10.1139/t00-027

Skempton, A. W. and J. M. Brogan. 1994, "Experiments on piping in sandy gravels." *Géotechnique* 44, no. 3: 449-460. https://doi.org/10.1680/geot.1994.44.3.449

Stevenson, R. and E. Bowman. 2025, "Effective Stress and Suffusion Onset at Local and Global Scales in Centrifuge Permeameter Tests." *Journal of Geotechnical and Geoenvironmental Engineering* 151, no. 2. https://doi.org/10.1061/jggefk.Gteng-13169

Taylor, R. N. 1994. *Geotechnical centrifuge technology*, 1st London: CRC Press. https://doi.org/10.1201/9781482269321

Terzaghi, K., R. B. Peck, and G. Mesri. 1995. *Soil mechanics in engineering practice*, 3rd United States: John Wiley.

Thusyanthan, I. and S. P. G. Madabhushi, 2003, "Scaling of seepage flow velocity in centrifuge models," Geotechnical and Environmental Research Group, University of Cambridge, London.

van Beek, V. M. and A. Zwanenburg. 2010. "Piping: Centrifuge experiments on scaling effects and levee stability." In *Physical Modelling in Geotechnics, Two Volume Set*, edited by S. Springman, J. Laue, and L. Seward, 183-189. Zurich: CRC Press. https://doi.org/10.1201/b10554

van Tonder, W. D. and S. W. Jacobsz. 2017, "Seepage column hydraulic conductivity tests in the geotechnical centrifuge." *Journal of The South African Institution of Civil Engineering* 59, no. 3: 16-24. https://doi.org/10.17159/2309-8775/2017/v59n3a3

Wang, Q., Z. Chen, Y. Jin, and J. Liang. 2010. "Development of a circulating system for water supply in centrifuge model tests." In *Physical Modelling in Geotechnics, Two Volume Set*, edited by J. L. Sarah Springman, Linda Seward, 285-289. Zurich, Switzerland: CRC Press. https://doi.org/10.1201/b10554

Wang, X., D. Ling, Y. Tang, T. Hu, Z. Gao, and Y. Chen. 2024, "Hydraulic heave in granular soils under hypergravity conditions." *Powder Technology* 440, no. 1: 119764. https://doi.org/10.1016/j.powtec.2024.119764

Zhang, L. M., Y. Xu, and J. S. Jia. 2009, "Analysis of earth dam failures: A database approach." *Georisk: Assessment and Management of Risk for Engineered Systems and Geohazards* 3, no. 3: 184-189. https://doi.org/10.1080/17499510902831759

Zornberg, J. G. and J. S. McCartney. 2010, "Centrifuge Permeameter for Unsaturated Soils. I: Theoretical Basis and Experimental Developments." *Journal of Geotechnical and Geoenvironmental Engineering* 136, no. 8: 1051-1063. https://doi.org/10.1061/(ASCE)GT.1943-5606.0000319

Table 1 Overview of geotechnical centrifuge apparatuses related to seepage and internal erosion soil column tests

Apparatus	Maximum acceleration reported by authors	Water supply	Water level control	Flow rate measurement	Soil column tests		
					Axial stress controllability	Hydraulic gradient measurement	Applications
Singh and Gupta, 2000	200 *g*	Discontinuous, via fall head method	Unstable and uncontrollable	Indirect, via the descent rate of water level	No	No	Permeability
van Tonder and Jacobsz, 2017	23 *g*				No	Yes	
Ovalle-Villamil and Sasanakul, 2018 and 2020	30 *g*	Continuous, via pneumatic tanks outside of the swinging basket and two centrifuge water lines	Unstable but controllable	Indirect, via the displacement rate of pneumatic tank pistons	No	Yes	Permeability and heave
Zornberg and McCartney, 2010	400 *g*	Continuous, via a pump outside of the swinging basket and centrifuge water lines	Unstable but controllable	Direct, via outflow transducers in the swing basket	No	Yes	Permeability of unsaturated soils
Marot et al, 2012	40 *g*	Continuous, via a pump in the swinging basket	Stable, via overflow, but uncontrollable	No	No	No	Suffusion
Stevenson and Bowman, 2025	40 *g*	Discontinuous, via a pressurized supply tank	Stable, via overflow, and controllable, via a servo upstream lifting system	Indirect, via the ascent rate of a collection tank water level	No	Yes	Suffusion
van Beek and Zwanenburg, 2010	80 *g*	Continuous, via a pump in the swinging basket	Stable, via overflow, and controllable, via a plunger	No	Not applicable		
Wang et al, 2010	30 *g*	Continuous, via a pump in the swinging basket	Stable, via overflow but uncontrollable	Indirect, via a triangular weir	Not applicable		
Shepley and Bolton, 2013	60 *g*	Continuous, via water source outside of the swinging basket and one centrifuge water line	Stable and controllable, via a manual flow-control valve outside of the swinging basket	Direct, via a turbine flowmeter outside of the swinging basket	Not applicable		
CASIE	80 *g*	Continuous, via a pump in the swinging basket	Stable, via overflow, and controllable, via a servo upstream lifting system	Direct, via oval gear flowmeters in swinging basket	Yes	Yes	Permeability, heave, and suffusion

Table 2 Calibration results of flowmeters

The slope of sensitivity at N g to 1 g, K_N/K_1		Centrifugal acceleration, N: g			
		10	30	50	80
Flowmeter	10-100 ml/min	1.065	1.094	1.156	N/A
	30-300 ml/min	1.051	1.121	1.183	1.178
	100-1000 ml/min	1.063	1.059	1.070	1.087
	800-10000 ml/min	1.095	1.101	1.041	1.098
Average		1.068	1.093	1.109	1.120

Table 3 Soil properties

Soil Properties	
Specific gravity	2.662
Fine particle ratio: %	30
Maximum void ratio	0.775
Minimum void ratio	0.351
Target relative density: %	90
Effective particle size, d_{eff}: mm	0.253
Uniformity coefficient	13.3
Coefficient of curvature	7.44
Unified Soil Classification System (ASTM, 2025)	SP
$(H/F)_{\min}$ (Kézdi, 1979)	0 < 1 (unstable)
$(D_{15c}/d_{85f})_{\max}$ (Kenney and Lau, 1985)	9.49 > 4 (unstable)
Conditional factors of uniformity (Burenkova, 1993)	h'=1.34; h''=17.1 $0.67\lg(h'')+1=1.83> h'$ (unstable)

Figure 1 Schematic diagram of CASIE

Figure 2 Photograph of CASIE

Figure 3 Applications of permeameter: (a) a typical layout of permeability tests under downward flow; (b) the layout of heave tests; (c) a typical layout of suffusion tests under constant axial stress and downward flow; (d) a typical layout of suffusion tests under constant volume and upward flow

Figure 4 Pressure measurement unit: (a) 3D view; (b) sectional view of one three-way connector

Figure 5 Capability of centrifugal pump in the hypergravity environment

Figure 6 Operation principle of oval gear flowmeter: input cell (marked as I), output cell (O), and temporary water-carrying cell (T)

Figure 7 Schematic diagram of the flowmeter calibration method: falling head method using upstream water tank

Figure 8 Performance of oval gear flowmeters in the hypergravity environment

Figure 9 Particle size distribution

Figure 10 Applied hydraulic path for suffusion test at 30 *g*

Figure 11 Suffusion evolution at 30 *g*: (a) hydraulic gradient; (b) flowrate

Figure 12 Photographs of the erosion process at 30 *g*: (a) before the test, homogeneous fine particle distribution; (b) 30*g*-2, coarse particles becoming visible; (c) 30*g*-3, small pure coarse sand regions; (d) 30*g*-5, expanded pure coarse sand regions

Figure 13 Suffusion evolution at 1 *g*: (a) hydraulic gradient; (b) flowrate

Figure 14 Velocity versus hydraulic gradient: (a) 30 *g*; (b) 1 *g*

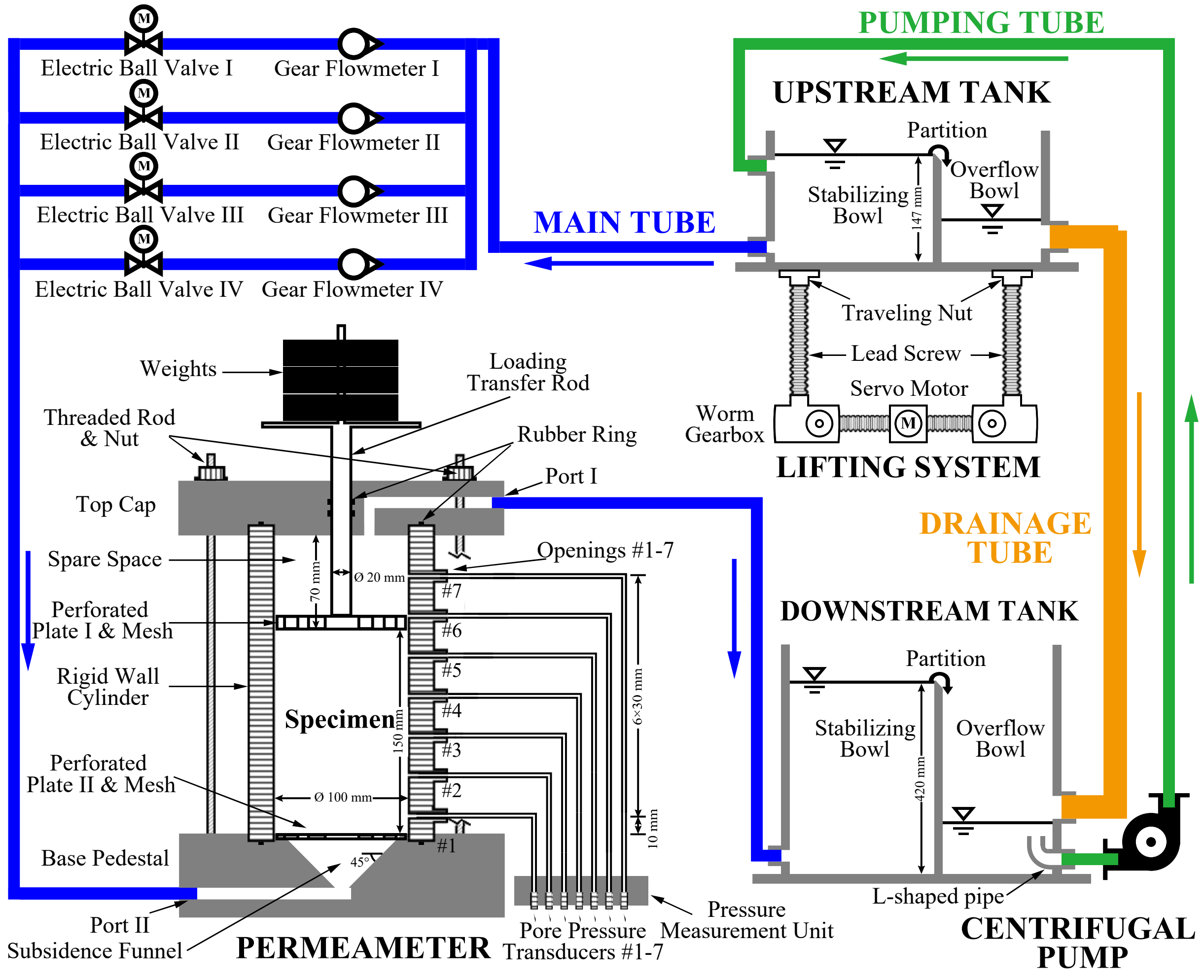

Figure 1 Schematic diagram of CASIE

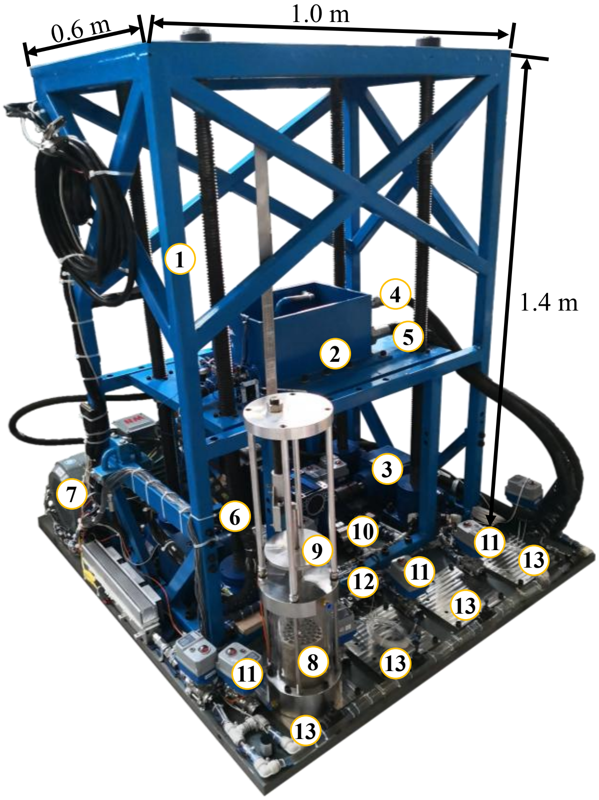

1.	Steel frame
2.	Upstream water tank
3.	Motor and gear box
4.	Pumping tube
5.	Drainage tube
6.	Main tube
7.	Centrifugal pump
8.	Permeameter
9.	Weights
10.	Gear flowmeters
11.	Electric ball valves
12.	Pressure measurement unit
13.	Baseplates for installing permeameters

Figure 2 Photograph of CASIE

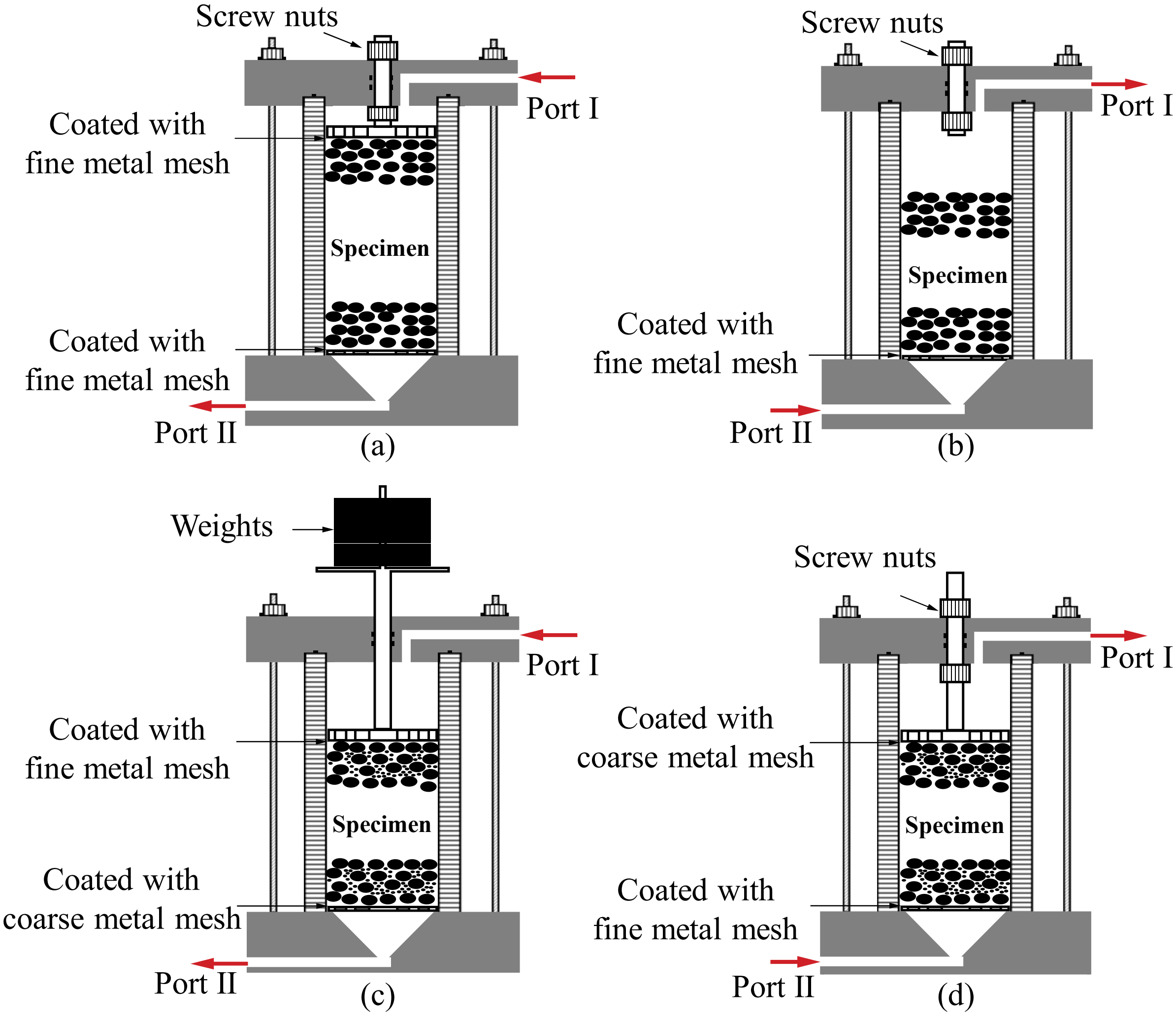

Figure 3 Applications of permeameter: (a) a typical layout of permeability tests under downward flow; (b) the layout of heave tests; (c) a typical layout of suffusion tests under constant axial stress and downward flow; (d) a typical layout of suffusion tests under constant volume and upward flow

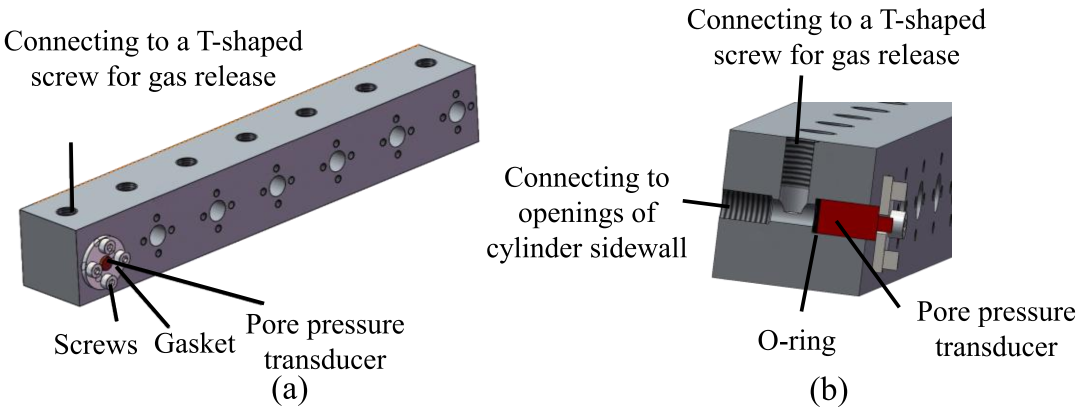

Figure 4 Pressure measurement unit: (a) 3D view; (b) sectional view of one three-way connector

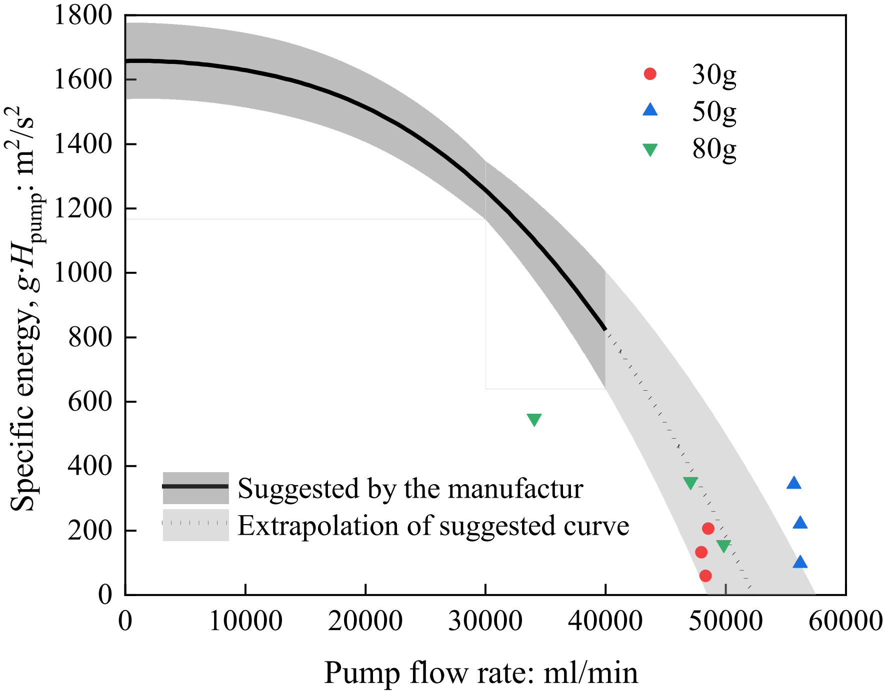

Figure 5 Capability of centrifugal pump in the hypergravity environment

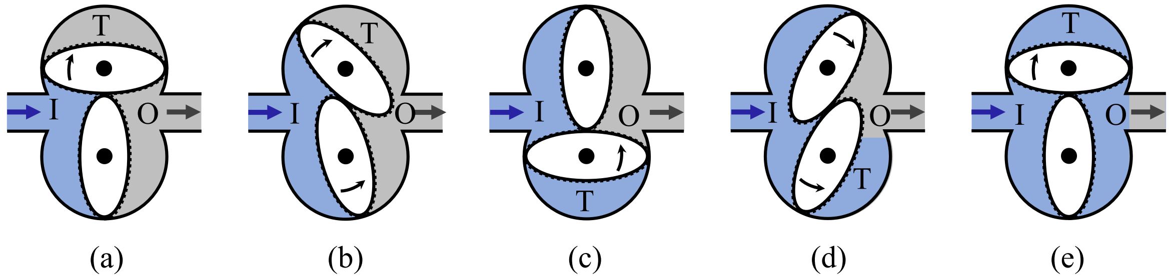

Figure 6 Operation principle of oval gear flowmeter: input cell (marked as I), output cell (O), and temporary water-carrying cell (T)

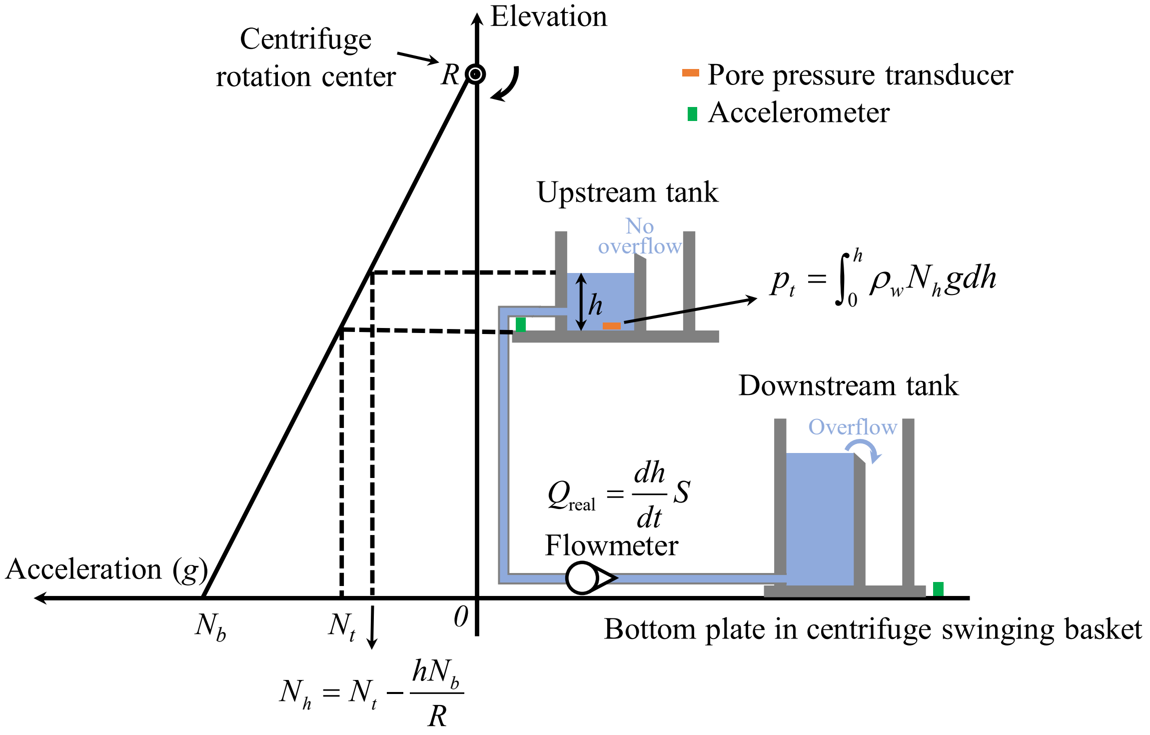

Figure 7 Schematic diagram of the flowmeter calibration method: falling head method using upstream water tank

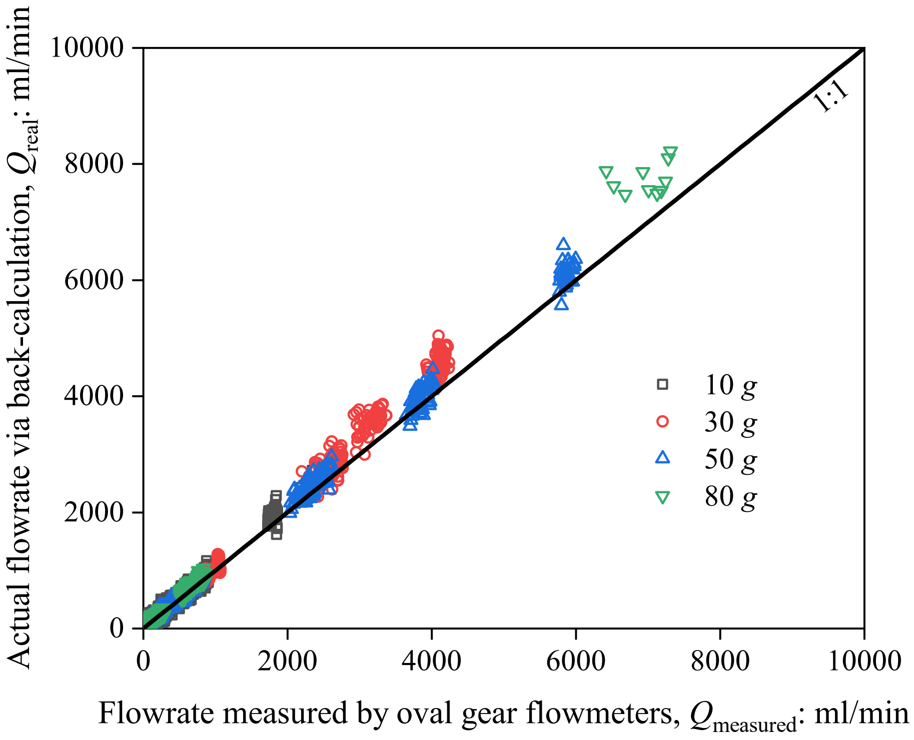

Figure 8 Performance of oval gear flowmeters in the hypergravity environment

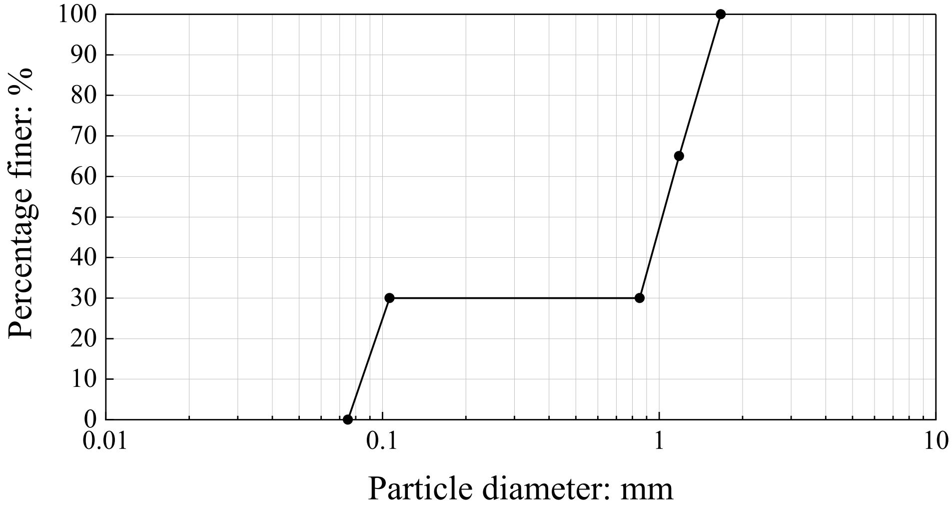

Figure 9 Particle size distribution

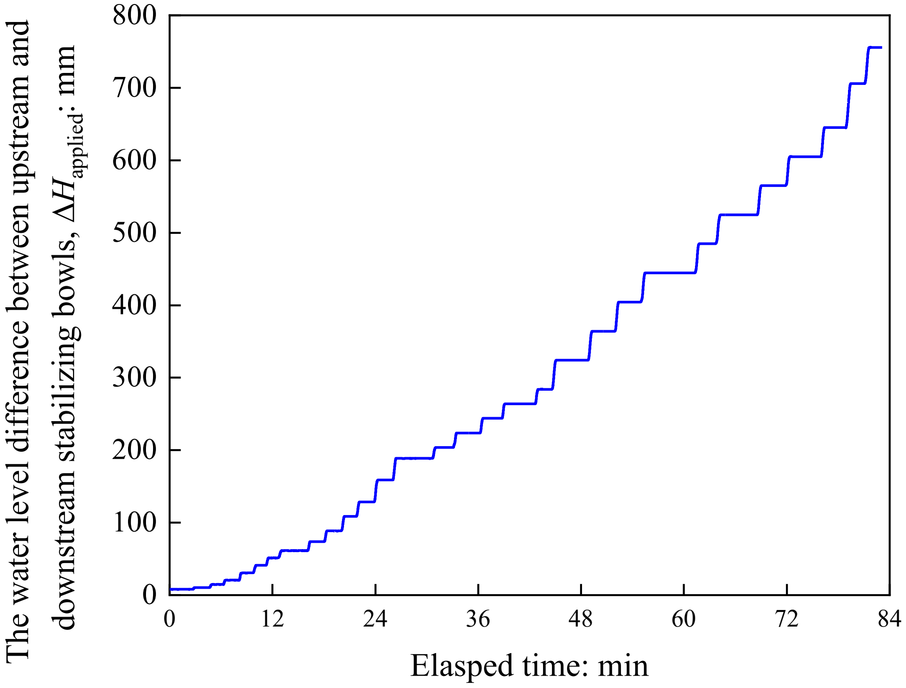

Figure 10 Applied hydraulic path for suffusion test at 30 *g*

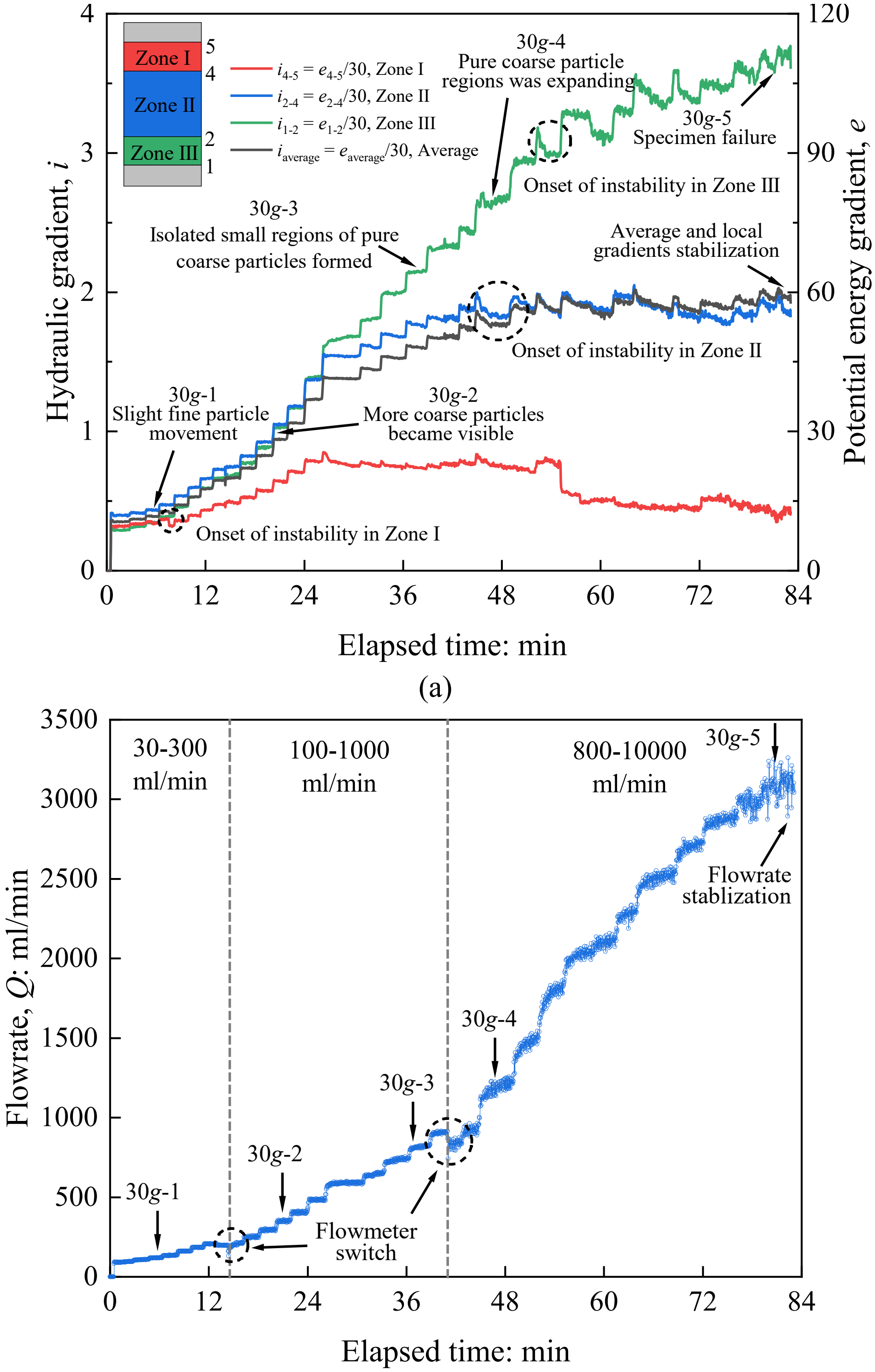

(a)

(b)

Figure 11 Suffusion evolution at 30 *g*: (a) hydraulic gradient; (b) flowrate

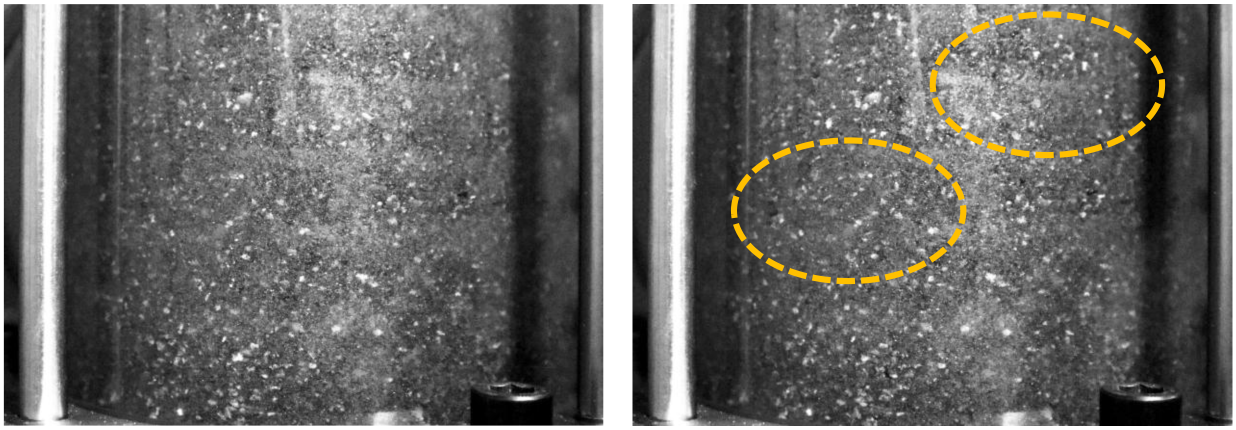

(a) Before the test, $i_{\text{average}} = 0$

(b) 30*g*-2, 21 min, $i_{\text{average}} = 0.94$

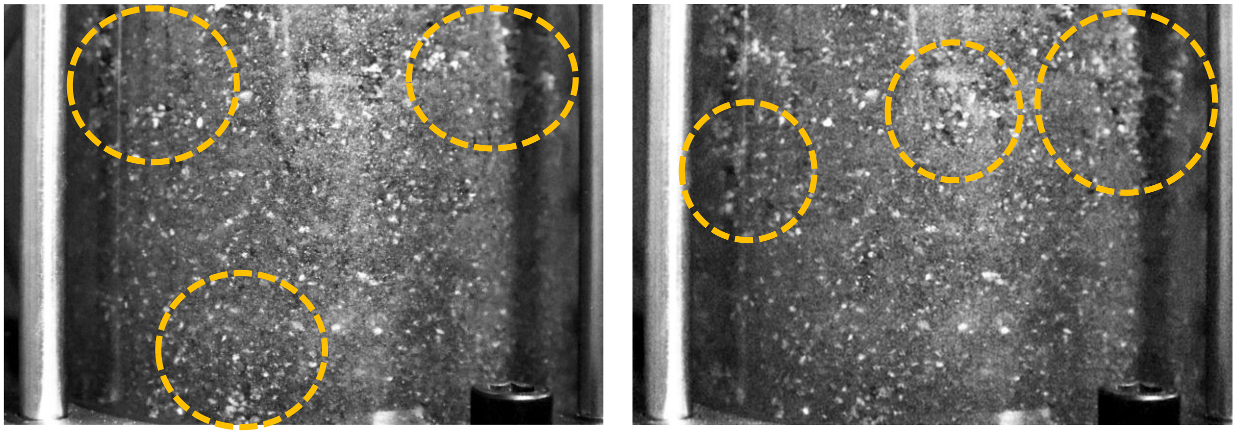

(c) 30*g*-3, 37 min, $i_{\text{average}} = 1.60$

(d) 30*g*-5, 81min, $i_{\text{average}} = 1.98$

Figure 12 Photographs of the erosion process at 30 *g*: (a) before the test, homogeneous fine particle distribution; (b) 30*g*-2, coarse particles becoming visible; (c) 30*g*-3, small pure coarse sand regions; (d) 30*g*-5, expanded pure coarse sand regions

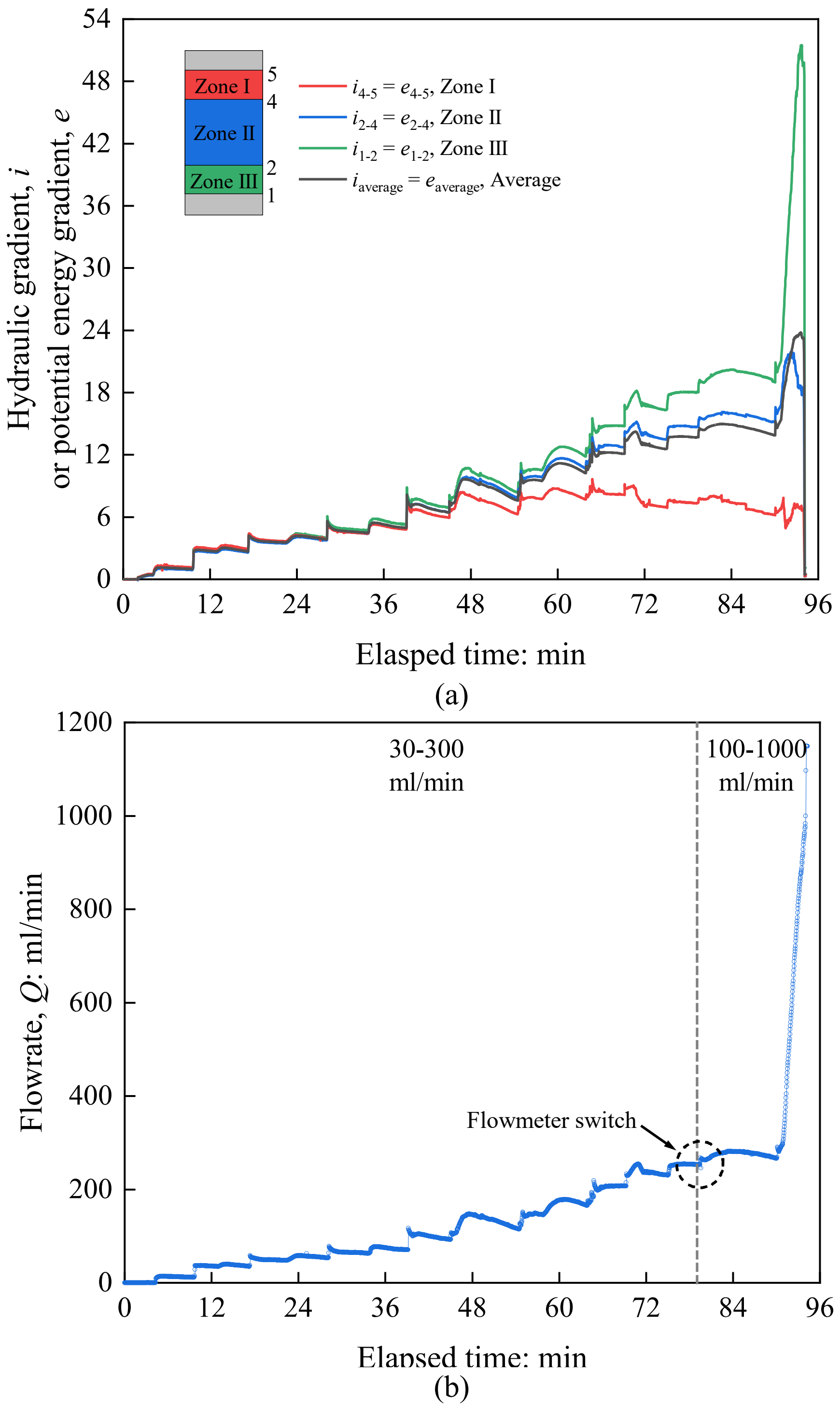

Figure 13 Suffusion evolution at 1 *g*: (a) hydraulic gradient; (b) flowrate

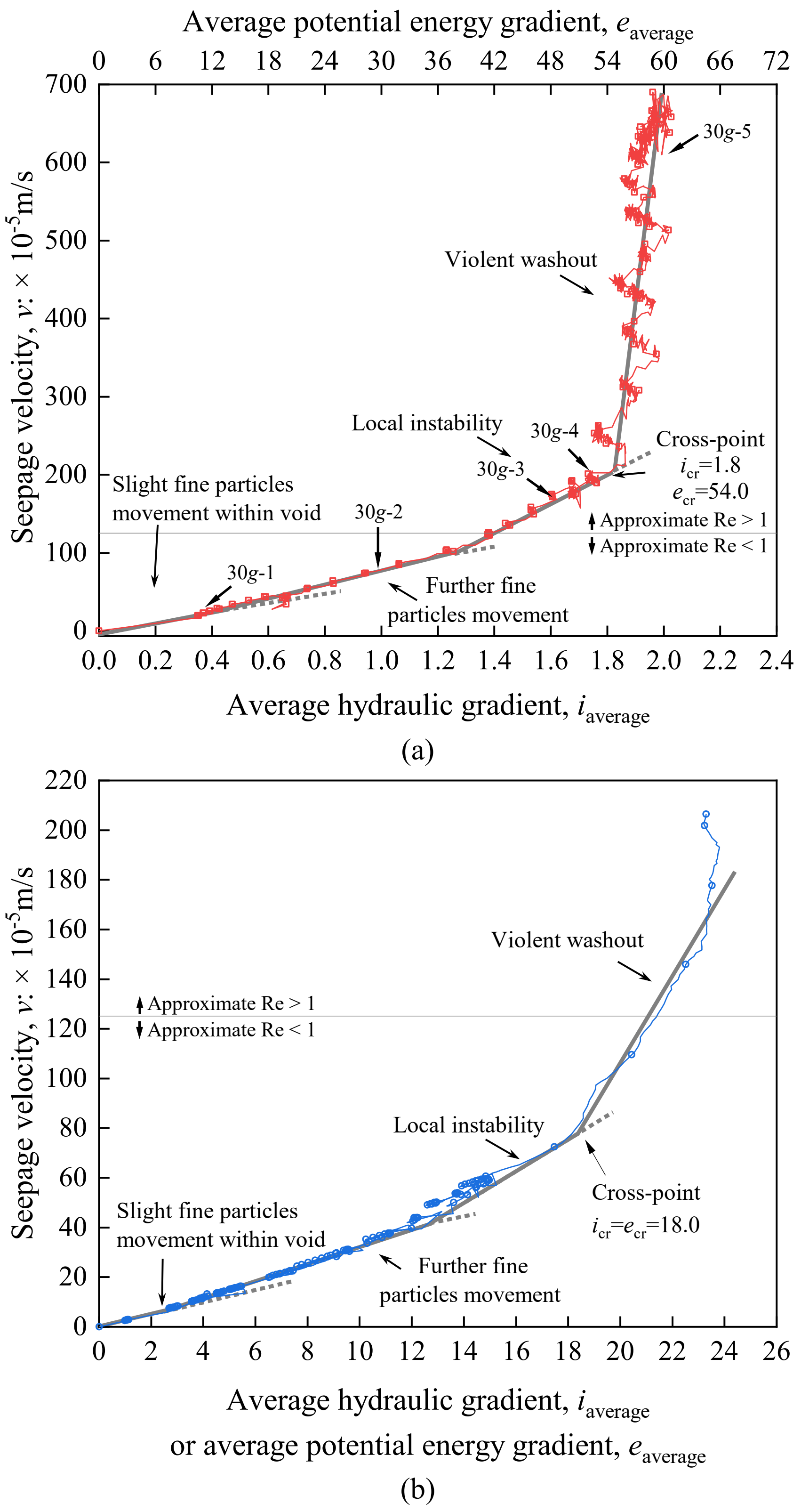

Figure 14 Velocity versus hydraulic gradient: (a) 30 *g*; (a) 1 *g*